I2MTC paper #98 (1570780459)

Enhanced IpD2FT-based Synchrophasor Estimation for M Class PMUs through Adaptive Narrowband Interferers Detection and Compensation

Xuansheng Shan, *Student Member, IEEE*, David Macii, *Senior Member, IEEE,* Dario Petri, *Fellow, IEEE,* and *He Wen, Senior Member*

***Abstract*—One of the most challenging problems in the design of next-generation Phasor Measurement Units (PMUs) is related to the need to minimize the impact of multiple harmonics and out-of-band interharmonics (OOBI) on the measurement of synchrophasors over short observation intervals. Most of the existing solutions aim at removing such narrowband disturbances before synchrophasor estimation. However, when data records are short, accurate OOBI filtering may be infeasible. The algorithm described in this paper tackles this problem through a prior estimation of the number and the frequency of the significant narrowband interferers emerging from the noise floor. This result is achieved using a non-parametric signal detector based on random matrix theory and hypothesis testing, followed by the application of the estimation of signal parameters via the rotational invariance technique (ESPRIT). Once the number and the frequency of the narrowband components are known, these parameters are used to augment the dimension of the frequency-domain linear system of equations employed by the Interpolated Dynamic Discrete Fourier Transform (IpD2FT) for synchrophasor estimation. The results of multiple simulations confirm not only that the proposed approach for narrowband components detection is robust and more accurate than other model-order estimation algorithms described in the scientific literature, but also that the synchrophasor estimation accuracy over two-cycle observation intervals is generally higher than using other for M Class PMUs algorithms when OOBIs or a mixture of OOBIs and harmonics are considered**.

***Index Terms*—Phasor Measurement Units (PMUs), model order detection, ESPRIT, Discrete Fourier Transform (DFT).**

Xuansheng Shan (e-mail: shanxs006@hnu.edu.cn) is with the College of Electrical and Information Engineering, Hunan University, Changsha, Hunan Province, 410082, China. Currently, he is also a visiting Researcher at Department of Industrial Engineering, University of Trento, Trento, 38123, Italy (xuansheng.shan@unitn.it)

David Macii (e-mail: david.macii@unitn.it) and Dario Petri (e-mail: dario.petri@unitn.it) are with the Department of Industrial Engineering, University of Trento, Trento, 38123, Italy.

He Wen (e-mail: he_wen@hnu.edu.cn) is with the College of Electrical and Information Engineering, Hunan University, Changsha, Hunan Province, 410082, China.

This work is partly funded by the China Scholarship Council, the National Key Research and Development Program of China under Grant 2020YFC2004003 and Grant 2020YFC2004002, the National Natural Science Foundation of China under Grant 61771190, and the Hunan Provincial Natural Science Foundation of China under Grant 2019JJ20001.

I. Introduction

With the widespread diffusion of both renewable energy sources and increasingly nonlinear loads (e.g., plug-in electric vehicles and high-efficiency heat pumps), the voltage and current waveforms in power systems may exhibit a relevant harmonic and interharmonic content. Such narrowband interferers (especially the so-called out-of-band interferers - OOBIs and the low-order harmonics) can seriously affect synchrophasor magnitude and phase measurement, as well as fundamental frequency and Rate of Change of Frequency (ROCOF) estimation. From this standpoint, the existing digital estimation algorithms for Phasor Measurement Units (PMUs) can be roughly divided into two broad categories, i.e., the techniques that filter or remove such disturbances prior to synchrophasor estimation and those that instead estimate the parameters of the narrowband disturbances to mitigate their impact on the estimation of the fundamental synchrophasor. Such a classification and a list of some existing methods belonging to either category is reported in Table I.

The former kind of methods are more common and they usually rely on simpler and less computationally intensive algorithms, since they do not need to include narrowband components in the signal model. For instance, many commercial PMUs rely on the down-conversion of the spectrum of the acquired waveform around DC, followed by digital low-pass filtering. This approach is often called Down-conversion and Filtering (DCF) and it is also mentioned in Annex D of the IEEE/IEC Standard 60255-118-1:2018 [1] (in the following simply referred to as the IEEE/IEC Standard). The accuracy of DCF techniques strongly depends on the selectivity of the chosen low-pass filters. Linear-phase digital filters can be designed to ensure a narrow transition bandwidth and a high OOBIs and low-order harmonics attenuation. For instance, a conservative low-pass filter design criterion was proposed in [2]. Similarly, adaptive filtering techniques based on fundamental frequency estimation may strongly mitigate the impact of harmonics [3]. However, when linear-phase filters are considered, a delicate tradeoff exists between PMU passband flatness (required to track possible amplitude and phase fluctuations of the fundamental component), OOBI rejection capability and filter responsiveness [4] In particular, higher filter selectivity requires longer impulse response, which may cause an unacceptable latency.

TABLE I
CLASSIFICATION OF DIFFERENT PMU ALGORITHMS ABOUT THEIR ABILITY TO MITIGATE THE IMPACT OF HARMONIC AND INTER-HARMONIC INTERFERERS.

Category	Methods	Pros	Cons
Canceling the interferers	DCF [1,2]	Low computational complexity	Long latency required to achieve OOBI rejection
	Windowed IpDFT [5-7]		
	IpD2FT [13]	Dynamic signal model	
	Disturbances whitening [14]	Short observation intervals, good harmonic rejection performance	OOBI rejection performance not investigated
Estimating the interferers	TLTFT [16]	Dynamic signal model, model extension based on limited number of harmonics	Unable to mitigate OOBIs
	IpDFTc [17]	Low computational complexity	Static signal model, unable to mitigate OOBIs
	i-IpDFT [18]		Static signal model, empirically tuned threshold for the narrowband components detection
	ESPRIT+TFT [22,24]	Dynamic signal model, OOBIs well mitigated	Empirically tuned threshold for the narrowband components detection
	MP+TFT [23]		
	CS-TFT [25,26]		Observation of at least three powerline cycles

The techniques based on the basic Discrete Fourier Transform (DFT) or the Interpolated DFT (IpDFT) exhibit similar limitations [5-7]. In fact, such algorithms are computationally lightweight and they may strongly mitigate the impact of possible stationary narrowband interferers [8], provided that the effect of possible off-nominal frequency deviations is compensated properly [9], and that both spectral picket-fence and leakage effects are restrained, e.g., through suitable windowing of the input data record [10, 11]. In fact, the effectiveness of window functions on OOBIs can be severely impaired when observation intervals shorter than about three nominal cycles are considered [12]. This problem affects also the Interpolated Dynamic DFT (IpD2FT) algorithm [13], despite its better ability to track synchrophasor variations over time. In [14], a totally different approach for narrowband components removal is proposed. Indeed, such disturbances are whitened (i.e. transformed into wideband noise) before estimating the synchrophasor parameters through a Taylor–Kalman filter. Although disturbance whitening is particularly effective in improving accuracy over short observation intervals, its OOBIs rejection capability (which is essential for M Class PMUs) has not been investigated, yet.

The enhanced IpD2FT (eIpD2FT) algorithm described in this paper is an improved version of the algorithm initially presented at the I2MTC 2022 conference [15]. While it partially relies on the same theoretical background in [14], it is based on a totally different perspective, i.e., estimating the parameters of possible narrowband interferers, rather than filtering or removing them. Therefore, the eIpD2FT algorithm belongs to the second category of estimators shown in Table I. A further advantage of such methods is that the estimated parameters can be exploited for other purposes than phasor parameters measurement (e.g., power quality monitoring or grid-level harmonic state estimation).

A deeper qualitative analysis of the key features and the novelty of the eIpD2FT algorithm with respect to other estimators based on the same underlying rationale is explained in Section II. Section III describes the details of the algorithm, while Section IV at first reports some results about the probability of correct detection of multiple narrowband components and then summarizes the estimator performances considering not only the M Class testing conditions specified in the IEEE/IEC Standard, but also a mixture of harmonics and interharmonics affecting the fundamental. Such results are compared with those obtained using both the original IpD2FT estimator and the Tuned Lightweight Taylor Fourier Transform (TLTFT) [16]. Finally, Section V concludes the paper.

II. RELATED WORK ON PMU ESTIMATION ALGORITHMS BASED ON MULTITONE PARAMETERS ESTIMATION

The idea of estimating the parameters of possible narrowband interferers affecting the fundamental synchrophasor is not new, although it is less common than the solutions described in Section I, which are conceived to filter harmonic and interharmonic disturbances.

A pair of IpDFT-based solutions that aim at estimating and compensating the detrimental effect of possible narrowband disturbances are the Corrected IpDFT (IpDFTc) [17] and the iterative IpDFT (i-IpDFT) algorithm [18]. Both techniques rely on a static synchrophasor model and mitigate the spectral interference produced by the negative image of the fundamental tone and the most critical narrowband components. While the IpDFTc does not compensate for the effect of possible OOBIs, the i-IpDFT addresses this problem, but it relies on an empirically tuned threshold for narrowband interferers detection, which may exhibit unexpected robustness issues if the Signal-to-Noise Ratio (SNR) is low. The eIpD2FT algorithm described in this paper relies instead on a phasor dynamic model and includes the narrowband components that emerge from the noise floor with a level of confidence that is almost independent of the actual SNR value.

One of the most famous PMU algorithms that includes the estimation of multiple narrowband components is the Taylor-Fourier Transform (TFT) [19]. The TFT extends the Taylor's based dynamic phasor model of the fundamental (initially presented in [20]) to the case of harmonic phasors. Also, the TFT was further optimized and enhanced in the case of three-phase signals [21]. In the TFT estimator, the phasors of both the fundamental component and a given number of harmonics are regarded as dynamic quantities and the variations of each of them over time are described by the Taylor's series of each phasor truncated to a specified order.

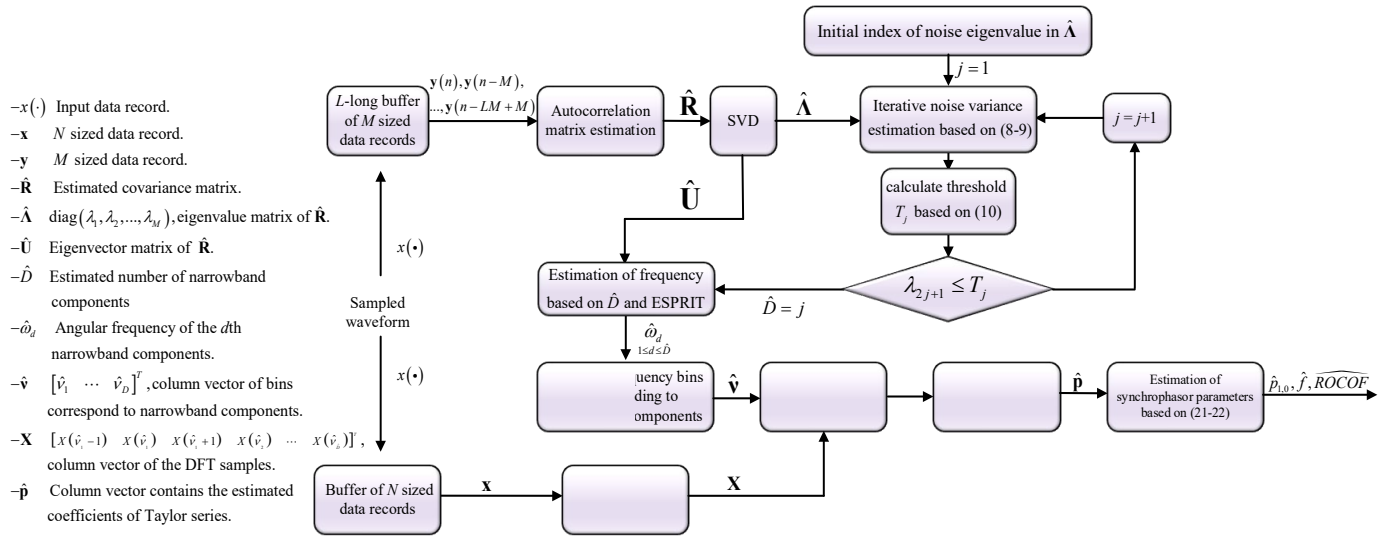

Fig. 1. Flow chart of the eIpD2FT algorithm

The Taylor's series coefficients (and consequently the synchrophasor amplitude and phase) are then estimated by finding the least-squares solution of an overdetermined linear system resulting from the expression that relates the time domain model of the signal to the record of acquired samples. Unfortunately, the performance of the original TFT degrades when the frequency of the fundamental differs from its nominal value. Moreover, the basic TFT does not include the interharmonics into the signal model since their number and their frequencies are completely unknown.

Various techniques based on signal and noise subspace decomposition can be used to estimate the frequency of multi-tone disturbances so enabling TFT accuracy improvement [22-24]. Among them, the multiple signal classification (MUSIC), the estimation of signal parameters via rotational invariant techniques (ESPRIT) or the matrix pencil method can be used. Unfortunately, a wrong model order selection may severely degrade the TFT estimation accuracy.

In [16] it was heuristically observed that the estimation accuracy degradation can be avoided if the fundamental frequency is properly estimated and an appropriate window function is used to weigh the input data record. Also, a very limited number of harmonics (depending on the observation interval length) should be included in the TFT signal model. Nonetheless, also in this case the lack of knowledge on possible OOBIs leads to poor performance, unless reasonably long observation intervals are considered.

The Compressive Sensing Taylor-Fourier Multifrequency technique [25] (recently extended for harmonics estimation [26]) tackles this problem and provides good OOBI detection capability and high frequency and synchrophasor estimation accuracy. Nonetheless, also this technique apparently requires the observation of at least three power line cycles to counteract the effect of large OOBIs.

Compared the TFT-based solutions mentioned above, and the preliminary eIpD2FT version presented in [15], the eIpD2FT estimator described in this paper has a key advantage, i.e., it can estimate the actual number of narrowband components with a high level of confidence through a non-parametric hypotheses testing algorithm based on random matrix theory. As a consequence, the detection of possible narrowband components is particularly robust and the synchrophasor estimation results obtained by augmenting the linear systems of equations of the original IpD2FT estimator exhibits high accuracy over two-cycle-long observation intervals even under the effect of both harmonics and OOBIs. To the best of Authors' knowledge, this is an unprecedented achievement.

III. EIPD2FT ALGORITHM DESCRIPTION

The multitone eIpD2FT estimation algorithm consists of three main steps, i.e.

1. Non-parametric estimation of the number of stationary narrowband components;
2. Estimation of fundamental, harmonic and interharmonic frequencies based on ESPRIT [27];
3. Fundamental, harmonics and interharmonics synchrophasor estimation through the IpD2FT algorithm [13].

Steps 1 and 2 rely on the same well-established theoretical framework, namely on the decomposition of the vector space of PMU signals into two orthogonal subspaces related to narrowband components and broadband noise, respectively. The underlying theoretical background is recalled in Section III.A. The algorithm for detecting the number of stationary narrowband components (which is essential to ensure high-accuracy results in steps 2 and 3) is described in Section III.B and it represents a major advancement compared with the purely heuristic threshold-based approach used in [15]. The ESPRIT technique for the frequency estimation of all detected components is summarized in Section III.C. Section III.D is instead devoted to the description of a multi-tone implementation of the IpD2FT algorithm. Finally, in Section III.E the algorithm computational complexity is analyzed. Fig. 1 depicts the flowchart of the whole eIpD2FT algorithm.

A. General theoretical background

Let

$$x(n)=\sum_{d=1}^{D}A_d(n)\cos\left(2\pi\frac{f_d}{f_s}n+\varphi_d(n)\right)+\varepsilon(n) \tag{1}$$

be the discrete-time sequence of a voltage or current waveform acquired by the PMU with sampling frequency f_s and consisting of both:

1. D narrowband components of amplitude, mean frequency and phase denoted as $A_d(n)$, f_d and $\varphi_d(n)$, respectively, for d=1,…,D (where d=1 refers to the fundamental term and D is unknown);
2. Broadband (i.e., almost white) normally distributed noise with zero mean and variance σ^2.

Observe that in (1) both $A_d(n)$ and $\varphi_d(n)$ are potentially time-varying quantities, i.e., they can be subjected to dynamic oscillations or sudden changes. Also, the term $\varphi_d(n)$ includes the effect of frequency variations around f_d. Considering that the PMU signals are digitized, the respective average normalized angular frequencies of the D narrowband components are $\omega_d=2\pi\frac{f_d}{f_s}$, for d=1,…,D. It is worth noting that the fundamental frequency f_1 may differ from the nominal value f_{nom} = 50 Hz or 60 Hz by a relative off-nominal frequency deviation in the order of a few per cent. According to the IEEE/IEC Standard, the angular rotation due to such possible off-nominal frequency deviations must be taken into account when the synchrophasor angle is estimated.

A sequence of $M > 2D$ consecutive samples of signal (1) can be rearranged into a column vector $\boldsymbol{y}(n)=\left[x(n)\;\; x(n+1)\;\; \ldots\;\; x(n+M-1)\right]^T$ where ^{T} denotes the transpose operator. In practice, $\boldsymbol{y}(n)$ can be rewritten as

$$\boldsymbol{y}(n)=\frac{1}{2}\mathbf{B}\mathbf{s}(n)+\boldsymbol{\varepsilon}(n) \tag{2}$$

where $\mathbf{B}=\left[\mathbf{E}(\omega_1)\;\; \mathbf{E}(\omega_2)\;\; \cdots\;\; \mathbf{E}(\omega_D)\right]$ is an $M\times 2D$ matrix with

$$\mathbf{E}(\omega_d)=\begin{bmatrix}1 & 1\\ e^{j\omega_d} & e^{-j\omega_d}\\ \vdots & \vdots\\ e^{j(M-1)\omega_d} & e^{-j(M-1)\omega_d}\end{bmatrix},\quad d=1,...,D, \tag{3}$$

$$\begin{aligned}\mathbf{s}(n)=[&A_1(n)e^{j(\omega_1 n+\varphi_1(n))}\quad A_1(n)e^{-j(\omega_1 n+\varphi_1(n))}\cdots\\ &A_D(n)e^{j(\omega_D n+\varphi_D(n))}\quad A_D(n)e^{-j(\omega_D n+\varphi_D(n))}]^T\end{aligned} \tag{4}$$

and $\boldsymbol{\varepsilon}(n)$ represents the vector of additive wideband noise samples. If the amplitude, phase and frequency fluctuations of the narrowband components are assumed to be negligible, recalling that $M > 2D$, the $M\times M$ autocorrelation matrix of $\boldsymbol{y}(n)$ can be decomposed as follows [27], i.e.

$$\mathbf{R}=E\left(\boldsymbol{y}(n)\boldsymbol{y}^T(n)\right)=\frac{1}{4}\mathbf{B}\mathbf{R}_D\mathbf{B}^H+\sigma^2\mathbf{I}_M \tag{5}$$

where $E(\cdot)$ and ^{H} denote the expectation and the Hermitian operator, respectively, $\mathbf{R}_D=\text{diag}\left(A_1^2, A_1^2, ..., A_D^2, A_D^2\right)$ is the $2D\times 2D$ autocorrelation matrix of the signal vector subspace including the D narrowband components, and $\mathbf{I}_M$ is the identity matrix (of size $M\times M$ in this case). If the Singular Value Decomposition (SVD) is applied to matrix $\mathbf{R}$, it results that

$$\begin{aligned}\mathbf{R}=\mathbf{U}\boldsymbol{\Lambda}\mathbf{U}^T&=\mathbf{U}\begin{bmatrix}\lambda_1 & \cdots & 0\\ \vdots & \ddots & \vdots\\ 0 & \cdots & \lambda_M\end{bmatrix}\mathbf{U}^T=\\ &=\begin{bmatrix}\mathbf{U}_D & \mathbf{U}_N\end{bmatrix}\begin{bmatrix}\frac{M}{4}\mathbf{R}_D+\sigma^2\mathbf{I}_{2D} & \mathbf{0}\\ \mathbf{0} & \sigma^2\mathbf{I}_{M-2D}\end{bmatrix}\begin{bmatrix}\mathbf{U}_D^T\\ \mathbf{U}_N^T\end{bmatrix}\end{aligned} \tag{6}$$

where $\boldsymbol{\Lambda}=\text{diag}\left(\lambda_1,...,\lambda_M\right)$ is the diagonal matrix including the singular values of $\mathbf{R}$, the columns of submatrices $\mathbf{U}_D$ and $\mathbf{U}_N$ of $\mathbf{U}$ are the orthonormal singular vectors associated, respectively, with the subspace including the narrowband components and with the noise subspace only. It is worth recalling that $\mathbf{R}$ is positive definite by construction. Hence, its singular values and eigenvalues actually coincide so that the columns of $\mathbf{U}$ are not only the singular vectors, but also the eigenvectors of $\mathbf{R}$. For this reason, the terms eigenvalues and singular values will be used interchangeably in the rest of this manuscript.

A closer analysis of $\boldsymbol{\Lambda}$ apparently suggests that in the case at hand the problem of estimating the number D of narrowband components has a straightforward solution. Indeed, by computing the ratio of pairs of consecutive eigenvalues (arranged in a non-ascending order as in (6)), the dimension of the narrowband components' subspace can be easily identified as soon as the ratio of consecutive singular values becomes equal to 1 twice in a row. Unfortunately, $\mathbf{R}$ in practice can be estimated by using a limited amount L of finite-length data records. As a consequence, the estimated singular values, arranged in a non-increasing order, exhibit a smoothed trend [28]. Thus, such values are different from the diagonal elements of $\boldsymbol{\Lambda}$ and the estimation of the number of narrowband components is inherently a stochastic problem, whose solution can be quite involved, as it will be explained in the next subsection.

B. Estimation of the number of narrowband components

The problem of detecting an unknown number of signals from noise is well-known in the scientific literature and it has been addressed with various techniques, most notably the Minimum Description Length (MDL) algorithm [29] and the Akaike Information Criterion (AIC) [30]. In the algorithm described in this paper, neither one of such common solutions is adopted, although their performance is reported for comparison in Section IV.A. The chosen approach relies instead on a slightly modified version of the estimation algorithm based on Random Matrix Theory (RMT) [28]. The rationale of this choice is threefold. Firstly, even if the MDL estimator is consistent when the number of observations L (i.e., the number of data records of the input signal (1)) tends to infinity, the detection threshold is larger than the asymptotic limit approximately by a factor $\sqrt{2\log L}$ [28]. Secondly, the MDL detection performance tends to drop as the Signal-to-Noise (SNR) ratio decreases [31]. In fact, the AIC detection accuracy is generally better than the MDL's one for low SNR values, but

the AIC estimator is not consistent [32]. Finally, neither the MDL, nor the AIC estimator are expected to perform very well when the number of data collected in each observation M is comparable with L [20]. This is instead the most likely scenario in the PMU case, since the value of M is limited by the number of samples that can be acquired within a few power line cycles, while L is constrained by both the computational burden and the detection latency. On the other hand, the RMT estimator is expected to offer a higher detection accuracy with a reasonable computational burden. Such expectations are indeed confirmed by the simulation results reported in Section IV.A. The RMT-based estimation relies on the maximum likelihood estimator of matrix **R,** i.e.

$$\hat{\mathbf{R}} = \frac{1}{L}\sum_{l=0}^{L-1} \boldsymbol{y}\left(n - l \cdot M\right) \boldsymbol{y}^T\left(n - l \cdot M\right). \quad (7)$$

Therefore, in practice the SVD is applied to (7) rather than to (5). Note that in $\hat{\mathbf{R}}$ the dependence on variable n is omitted because the acquired signal is assumed to be stationary. Furthermore, it is important to emphasize that the random matrix theory relies on the assumption that the elements of vectors $\boldsymbol{y}(\cdot)$ in (7) are all independent and identical distributed (i.i.d.). In the case at hand, this assumption holds true if the following two conditions are met, i.e.,

1. The data records collected by the PMU are not overlapped (which is a major difference compared with [15], where instead the L data records are shifted sample by sample and thus differ by just one sample at a time);
2. The initial phase angles of the D narrowband components in the L data records used to compute $\hat{\mathbf{R}}$ are uniformly distributed within [0, 2π).

The first condition arises from the fact that if the vectors of PMU data used to estimate $\hat{\mathbf{R}}$ are overlapped, then they are correlated too. In this case, the variance of the estimated eigenvalues of the noise subspace is expected to be larger than in the case when the vectors are i.i.d. Moreover, to the best of Authors' knowledge, no known probability density models exist at the moment to describe the stochastic distribution of the noise subspace eigenvalues estimated by using strongly correlated data, while instead this is possible when the data records are independent [33]. Therefore, if correlated observations are used, the threshold for signal detection could just be set heuristically (e.g., through Monte Carlo simulations), which however may pose serious robustness issues when the signal model parameters change unexpectedly. The main disadvantage of using nonoverlapped data records is the longer initial delay to detect the number of narrowband components. However, this is not a problem in quasi-stationary conditions if synchrophasor estimation is performed in parallel to narrowband components detection, as it will be described in Section III.D.

The second condition mentioned above is needed to properly estimate the autocorrelation of the D narrowband components. Indeed, they can be regarded as random processes only if their instantaneous phase angle is uniformly distributed within [0, 2π). In practice, to implement this condition by using the data collected over subsequent observation intervals, it is preferable to use records that are longer than a power line cycle and with duration M/fs that must not be a multiple of the period of any one of the components to be detected. Details of possible values are in fact reported in Section IV.

Following the same approach described in [28], the estimation of the number of narrowband components relies on an iterative hypothesis testing. In particular, if the M singular values of $\hat{\mathbf{R}}$ are computed and arranged in a descending order, the null and alternative hypotheses of the problem are:

- H_0: the $(2j+1)$-th singular value of $\hat{\mathbf{R}}$ does not exceed the threshold for narrowband components' detection, i.e., $\hat{\lambda}_{2j+1} \le T_j$;
- H_1: the $(2j+1)$-th singular value of $\hat{\mathbf{R}}$ exceeds the threshold for narrowband components' detection, i.e., $\hat{\lambda}_{2j+1} > T_j$;

where T_j is indeed the detection threshold computed in the j-th iteration of the algorithm itself. Such a threshold is proportional to the estimated variance of wideband noise, and it is updated in each iteration, as it will be explained in the following (see expression (10)).

Observe that the hypothesis testing considers only odd singular values, because real narrowband components always exhibit couples of singular values. Thus, if the null hypothesis is rejected for $\hat{\lambda}_{2j+1}$, it must be rejected for $\hat{\lambda}_{2j+2}$ too. Also, the null hypothesis is certainly rejected for $\hat{\lambda}_1$ since the fundamental component is always present in the application at hand. Therefore, the first pair of singular values can be skipped, and the algorithm is supposed to converge after D-1 iterations, i.e., as soon as the null hypothesis is accepted.

More in details, the steps of the RMT-based algorithm for the estimation of the number of narrowband components are summarized below.

1. First, singular values of $\hat{\mathbf{R}}$, namely the elements of matrix $\hat{\mathbf{\Lambda}} = \text{diag}\left(\hat{\lambda}_1, ..., \hat{\lambda}_M\right)$ are computed and arranged in a descending order.
2. Afterwards, starting from j=1, $\hat{D}$ is initialized to 1 and the variance of the noise floor is estimated to eventually compute T_j in step 3. As explained in Section III.A, all eigenvalues of the noise subspace should theoretically be equal to σ^2. Thus, a possible basic estimator of the noise variance is just the average of all eigenvalues that are assumed not to be related to the narrowband components, i.e., $\hat{\sigma}^2_{0|\hat{D}} = \frac{1}{M-2\hat{D}}\sum_{m=2\hat{D}+1}^{M} \hat{\lambda}_m$. Of course, if one or more of the singular values in the sum refers instead to some undetected narrowband component, is likely to be considerably greater than σ^2, which should lead to the rejection of hypothesis H_0. However, even if $\hat{D} = D$, it is shown in [34] that $\hat{\sigma}^2_{0|\hat{D}}$ is a biased estimator of σ^2, due to the limited size of the data records used to compute $\hat{\mathbf{R}}$. Thus, for a given value of $\hat{D}$, the following iterative estimator can mitigate the bias [28], i.e.,

$$\hat{\sigma}^2_{t|\hat{D}} = \frac{1}{M-2\hat{D}}\left[\sum_{m=1}^{M}\hat{\lambda}_m - \sum_{d=1}^{2\hat{D}}\rho_{d,t}\right] \quad (8)$$

where each coefficient $\rho_{d,t}$ is the largest real-valued solution of the second-degree algebraic equation

$$\rho^2_{d,t} - \rho_{d,t}\left[\hat{\lambda}_d + \hat{\sigma}^2_{t-1|\hat{D}}\left(1-\frac{M-2\hat{D}}{L}\right)\right] + \hat{\lambda}_d\hat{\sigma}^2_{t-1|\hat{D}} = 0\,. \quad (9)$$

In particular, the corrective terms given by (9) and used in (8) can compensate for the bias due to supposed $\hat{D}$ narrowband component [28, 34]. Observe that (9) depends on $\hat{\sigma}^2_{t-1|\hat{D}}$, i.e., on the noise variance estimated in the previous iteration, which can be initialized to $\hat{\sigma}^2_{0|\hat{D}}$. However, a few iterations (usually no more than 10) are enough to ensure that the $\hat{\sigma}^2_{t|\hat{D}}$ values returned by (8) converge to a constant value with fluctuations within ±1% [34].

A sign analysis of the discriminant of (9) reveals that real-valued solutions of (9) exist if $0 < \hat{\sigma}^2_{t-1|\hat{D}} \le \hat{\lambda}_d \Big/ \left(1+\sqrt{\frac{M-2\hat{D}}{L}}\right)^2$. This condition is generally met in practice if values of $\hat{\lambda}_d$ for d=1,…, $2\hat{D}$ are at least comparable with those of the noise floor variance.

3. Once the noise variance is estimated, the detection threshold is given by [28]:

$$T_j = \hat{\sigma}^2_{RMT|\hat{D}}\left(\mu_{L,M-2\hat{D}} + s(\beta)\xi_{L,M-2\hat{D}}\right) \quad (10)$$

where

$$\mu_{L,M-2\hat{D}} = \frac{1}{L}\left(\sqrt{L-\frac{1}{2}} + \sqrt{M-2\hat{D}-\frac{1}{2}}\right), \quad (11)$$

$$\xi_{L,M-2\hat{D}} = \sqrt{\frac{\mu_{L,M-2\hat{D}}}{L}}\left(\frac{1}{\sqrt{L-1/2}} + \frac{1}{\sqrt{M-2\hat{D}-1/2}}\right) \quad (12)$$

are the centering and scale parameters, respectively, of the probability density function of the ratio between the largest estimated noise subspace eigenvalue of $\hat{\mathbf{R}}$ and σ^2, while $s(\beta)$ represents the β-quantile of wrongly rejecting H_0, i.e., $F_{TW}\left(s(\beta)\right) = 1-\beta$ where,

$$F_{TW}(s) = \lim_{\substack{L,M\to\infty \\ \frac{M}{L}\to\text{const}}} \Pr\left\{\frac{\hat{\lambda}_{2D+1}/\sigma^2 - \mu_{L,M-2D}}{\xi_{L,M-2D}} \le s\right\} \quad (13)$$

is the Tracy-Widom cumulative distribution function and $\Pr\{\cdot\}$ is the probability operator [28]. Quite importantly, it is shown in [28, 35] that if $\beta << 1$ then

$$s(\beta) \approx \left(-\tfrac{3}{2}\log\left(4\sqrt{\pi}\beta\right)\right)^{\frac{2}{3}}. \quad (14)$$

4. Finally, the hypothesis testing is performed by comparing $\hat{\lambda}_{2j+1}$ with the threshold value given by (10). If the null hypothesis H_0 is rejected (namely if H_1 holds), then both index j and the value of $\hat{D}$ are incremented by 1 and the algorithm starts over from step 2; otherwise, the null hypothesis is supposed to be true and the algorithm ends. In this case, the number of detected narrowband components is $\hat{D} = j$. Quite importantly, if $\hat{D}$ is really equal to D, the noise variance estimator $\hat{\sigma}^2_{RMT|\hat{D}}$ based on (8) and (9) is almost unbiased, i.e. $E\left(\hat{\sigma}^2_{RMT|\hat{D}=D}\right) = \sigma^2 + O\left(\frac{1}{L^2}\right)$ [34].

C. Frequency estimation based on ESPRIT

If the amplitude, phase and frequency of the $\hat{D}$ narrowband components detected in the previous step are almost stationary, the ESPRIT algorithm can estimate the individual frequency values by using the same theoretical background described in Section III.A, as well as the shift invariance property of the periodic signals of the narrowband components' subspace [27]. In particular, if we denote with $\hat{\mathbf{U}}_{D1} = \left[\mathbf{I}_{M-1} \quad \mathbf{0}\right]\hat{\mathbf{U}}_D$ and $\hat{\mathbf{U}}_{D2} = \left[\mathbf{0} \quad \mathbf{I}_{M-1}\right]\hat{\mathbf{U}}_D$, the $(M-1)\times 2\hat{D}$ matrices consisting of rows from 1 to M−1 and from 2 to M of matrix $\hat{\mathbf{U}}_D$, respectively, it follows that $\hat{\mathbf{U}}_{D2} = \boldsymbol{\Psi}\hat{\mathbf{U}}_{D1}$, where $\boldsymbol{\Psi}$ is a rotation matrix because the columns of $\hat{\mathbf{U}}_{D1}$ and $\hat{\mathbf{U}}_{D2}$ are the singular vectors or eigenvectors of $\hat{\mathbf{R}}$ (namely pairs of quadrature sequences at different frequencies) shifted by just one time samples [15]. Thus, the rotation matrix can be estimated through linear regression as follows, i.e.,

$$\hat{\boldsymbol{\Psi}} = \left(\hat{\mathbf{U}}^T_{D1}\hat{\mathbf{U}}_{D1}\right)^{-1}\hat{\mathbf{U}}^T_{D1}\hat{\mathbf{U}}_{D2}\,. \quad (15)$$

The exponents of the eigenvalues of matrix $\hat{\boldsymbol{\Psi}}$ resulting from (15), properly arranged into matrix $\hat{\boldsymbol{\Omega}} = \text{diag}\left(e^{-j\hat{\omega}_1}, e^{j\hat{\omega}_1}, \ldots, e^{-j\hat{\omega}_{\hat{D}}}, e^{j\hat{\omega}_{\hat{D}}}\right)$ are the positive and negative normalized angular frequencies of the detected narrowband components.

D. IpD2FT algorithm extension

Let N be the length of each data record used for synchrophasor estimation. In practice, N is chosen in such a way that approximately and integer number of power line cycles (i.e., within the resolution of ±1 sample) is collected when the waveform fundamental frequency $f_1 = f_{\text{nom}}$. Therefore, N must be different from M, which instead, as explained in Section III.B, must be chosen in such a way that M/f_s is not a multiple of the period of any one of the narrowband components to be detected.

In the rest of this paper, without loss of generality, N is chosen as an odd number so that the synchrophasor, the frequency and the ROCOF of the fundamental component can be computed exactly in the center of each observation interval $n = -\frac{N-1}{2}, \ldots, \frac{N-1}{2}$. Also, the data records are assumed to be refreshed by one sample at a time.

As shown in Fig. 1, to limit the overall PMU estimation latency, the IpD2FT-based synchrophasor estimation can be run in parallel to the estimation of parameters $\hat{D}$ and $\hat{\omega}_d$ for d=1,…, $\hat{D}$ as described in Sections III.B and III.C. Until the

number of stationary narrowband components is available, the basic IpD2FT algorithm presented in [13] can be used for synchrophasor estimation in any case, although with reduced accuracy. This indeed equivalent to assume that $\hat{D}=1$ and $\hat{\omega}_1=\omega_{\text{nom}}$. Afterwards, when the number and the frequencies of other possible narrowband components are estimated, the IpD2FT estimator can be enhanced by including the phasors of the $\hat{D}$ detected components in the vector of unknowns and by using the values of normalized frequency $\hat{\omega}_d$ for d=1,…, $\hat{D}$ to tune the elements of the system matrix, as it will be explained more in detail in the rest of this Section.

In this regard, it is worth recalling that the dynamic behavior of the phasor of each narrowband component can be approximately described by its Taylor's series around the center of the considered data record and truncated to the K_h-th order term. Therefore, signal (1) can be rewritten as [13]:

$$x(n)\approx\frac{1}{2}\sum_{d=1}^{\hat{D}}\left[\sum_{k=1}^{K_h}\left(n^k p_{d,k}e^{j\omega_d n}+n^k p_{d,k}^{*}e^{-j\omega_d n}\right)\right]+\varepsilon(n) \qquad (16)$$

where $p_{d,k}=\frac{1}{k!}p_d^{(k)}\left(\frac{1}{f_s}\right)^k$ represents the k-th coefficient of the Taylor's series of the d-th narrowband component, $p_d^{(k)}$ is the k-th order derivative of $A_d(n)e^{j\varphi_d(n)}$ computed in the center of the collected data record and superscript "*" denotes the complex conjugate operator. In this paper, the Taylor's series order K_1 of the fundamental phasor is set to 2, in accordance with the original IpD2FT definition [13]. The Taylor's series order of all the other narrowband component is instead set to 0, because i) such disturbances are indeed assumed to be stationary even in the first two steps of the algorithm and ii) possible time-varying fluctuations of harmonics and OOBIs are expected to produce a negligible impact on the estimation accuracy of the fundamental parameters. Assuming, to a first approximation and for the sake of simplicity, that the wideband noise term $\varepsilon(\cdot)$ in (1) is negligible, the windowed Discrete-Time Fourier Transform (DTFT) of (16) normalized by the DC gain of the chosen window function is

$$\begin{aligned}X(\nu)&=\frac{1}{W_0(0)}\sum_{n=-\frac{N-1}{2}}^{\frac{N-1}{2}}x(n)w(n)e^{-j\frac{2\pi}{N}\nu n}\\&\approx\sum_{k=0}^{K_1}p_{1,k}W_k(\nu-\hat{\nu}_1)+p_{1,k}^{*}W_k(\nu+\hat{\nu}_1)\\&+\sum_{d=2}^{D}\left\{p_{d,0}W_0(\nu-\hat{\nu}_d)+p_{d,0}^{*}W_0(\nu+\hat{\nu}_d)\right\}\end{aligned} \qquad (17)$$

where variable ν denotes the normalized frequency expressed in bins, $\hat{\nu}_d=\hat{\omega}_d N/(2\pi)$ is the normalized estimated frequency of the dth narrowband component and

$$W_k(\nu)=\frac{1}{W_0(0)}\sum_{n=-\frac{N-1}{2}}^{\frac{N-1}{2}}n^k w[n]e^{-j\frac{2\pi}{N}\nu n}=\frac{j^k}{W_0(0)}\frac{d^k W}{d\omega^k}\bigg|_{\frac{2\pi}{N}\nu} \qquad (18)$$

is proportional to the kth derivative of the DTFT of the window function $w(\cdot)$. Note that, due to the even symmetry of usual window functions, (18) is purely real if k is even and purely imaginary if k is odd.

Expression (17) can be used to improve the estimation accuracy of the original IpD2FT algorithm. In particular, if the vector $\mathbf{p}$ including the unknown coefficients of the Taylor's series of the fundamental synchrophasor is augmented by adding the phasors of the other $\hat{D}-1$ detected narrowband disturbances, expression (17) can be rearranged in a matrix form as

$$\mathbf{X}=\mathbf{W}_P(\hat{\mathbf{v}})\mathbf{p}+\mathbf{W}_I(\hat{\mathbf{v}})\mathbf{p}^{*} \qquad (19)$$

where:

- $\mathbf{p}=\begin{bmatrix}p_{1,0} & p_{1,1} & p_{1,2} & p_{2,0} & \cdots & p_{D,0}\end{bmatrix}^T$;
- $\hat{\mathbf{v}}=\begin{bmatrix}\hat{\nu}_1 & \cdots & \hat{\nu}_D\end{bmatrix}^T$;
- $\mathbf{X}=\begin{bmatrix}X(\hat{\nu}_1-1) & X(\hat{\nu}_1) & X(\hat{\nu}_1+1) & X(\hat{\nu}_2) & \cdots & X(\hat{\nu}_D)\end{bmatrix}^T$ is the $(\hat{D}+2)$-long column vector comprising the DTFT samples computed at the estimated narrowband frequencies and two additional DTFT samples, located one bin below and one bin above $\hat{\nu}_1$, respectively;
- $\mathbf{W}_P(\hat{\mathbf{v}})$ and $\mathbf{W}_I(\hat{\mathbf{v}})$ are $(\hat{D}+2)\times(\hat{D}+2)$ matrices whose elements can be computed from (18) once the vector of frequency values estimated by ESPRIT is known, i.e.

$$\mathbf{W}_P(\hat{\mathbf{v}})=\begin{bmatrix}W_0(-1) & \cdots & W_2(-1) & W_0(\hat{\nu}_1-\hat{\nu}_2-1) & \cdots & W_0(\hat{\nu}_1-\hat{\nu}_D-1)\\W_0(0) & \cdots & W_2(0) & W_0(\hat{\nu}_1-\hat{\nu}_2) & \cdots & W_0(\hat{\nu}_1-\hat{\nu}_{\hat{D}})\\W_0(1) & \cdots & W_2(1) & W_0(\hat{\nu}_1-\hat{\nu}_2+1) & \cdots & W_0(\hat{\nu}_1-\hat{\nu}_{\hat{D}}+1)\\W_0(\hat{\nu}_2-\hat{\nu}_1) & \cdots & W_2(\hat{\nu}_2-\hat{\nu}_1) & W_0(0) & \cdots & W_0(\hat{\nu}_2-\hat{\nu}_{\hat{D}})\\\vdots & \vdots & \vdots & \vdots & \vdots & \vdots\\W_0(\hat{\nu}_{\hat{D}}-\hat{\nu}_1) & \cdots & W_2(\hat{\nu}_{\hat{D}}-\hat{\nu}_1) & W_0(\hat{\nu}_{\hat{D}}-\hat{\nu}_2) & \cdots & W_0(0)\end{bmatrix}$$

and

$$\mathbf{W}_I(\hat{\mathbf{v}})=\begin{bmatrix}W_0(2\hat{\nu}_1-1) & \cdots & W_2(2\hat{\nu}_1-1) & W_0(\hat{\nu}_1+\hat{\nu}_2-1) & \cdots & W_0(\hat{\nu}_1+\hat{\nu}_{\hat{D}}-1)\\W_0(2\hat{\nu}_1) & \cdots & W_2(2\hat{\nu}_1) & W_0(\hat{\nu}_1+\hat{\nu}_2) & \cdots & W_0(\hat{\nu}_1+\hat{\nu}_{\hat{D}})\\W_0(2\hat{\nu}_1+1) & \cdots & W_2(2\hat{\nu}_1+1) & W_0(\hat{\nu}_1+\hat{\nu}_2+1) & \cdots & W_0(\hat{\nu}_1+\hat{\nu}_{\hat{D}}+1)\\W_0(\hat{\nu}_2+\hat{\nu}_1) & \cdots & W_2(\hat{\nu}_2+\hat{\nu}_1) & W_0(2\hat{\nu}_2) & \cdots & W_0(\hat{\nu}_2+\hat{\nu}_{\hat{D}})\\\vdots & \vdots & \vdots & \vdots & \vdots & \vdots\\W_0(\hat{\nu}_{\hat{D}}+\hat{\nu}_1) & \cdots & W_2(\hat{\nu}_{\hat{D}}+\hat{\nu}_1) & W_0(\hat{\nu}_{\hat{D}}+\hat{\nu}_2) & \cdots & W_0(2\hat{\nu}_{\hat{D}})\end{bmatrix}$$

If equation (19) and its complex conjugate counterpart are combined into a single linear system, the Taylor's series coefficients of the phasors of all identified components can be simply estimated as follows, i.e.

$$\begin{bmatrix}\hat{\mathbf{p}}\\\hat{\mathbf{p}}^{*}\end{bmatrix}=\begin{bmatrix}\mathbf{W}_P(\hat{\mathbf{v}}) & \mathbf{W}_I(\hat{\mathbf{v}})\\\mathbf{W}_I^{*}(\hat{\mathbf{v}}) & \mathbf{W}_P^{*}(\hat{\mathbf{v}})\end{bmatrix}^{-1}\begin{bmatrix}\mathbf{X}\\\mathbf{X}^{*}\end{bmatrix}. \qquad (20)$$

Quite importantly, unlike the original IpD2FT algorithm, in this there is no need to solve (20) iteratively, as the static frequencies of the narrowband components, including the fundamental one, are estimated through ESPRIT.

Ultimately, the fundamental synchrophasor at a given reference time is simply $\hat{p}_{1,0}$, while the corresponding values of frequency and ROCOF can be estimated through [20]

$$\hat{f}_1=\frac{f_s}{2\pi}\frac{\text{Im}\{\hat{p}_{1,1}\hat{p}_{1,0}^{*}\}}{|\hat{p}_{1,0}|^2}+f_{\text{nom}}, \qquad (21)$$

$$\widehat{\mathrm{ROCOF}} = \frac{f_s^2}{\pi}\left[\frac{\mathrm{Im}\left\{\hat{p}_{1,2}\hat{p}_{1,0}^*\right\}}{\left|\hat{p}_{1,0}\right|^2} - \frac{\mathrm{Re}\left\{\hat{p}_{1,1}\hat{p}_{1,0}^*\right\}\mathrm{Im}\left\{\hat{p}_{1,1}\hat{p}_{1,0}^*\right\}}{\left|\hat{p}_{1,0}\right|^4}\right]. \quad (22)$$

Recalling that the results of both (21) and (22) are particularly sensitive to wideband noise [36], and that in any case the results at the output of the PMUs should be decimated prior to be transmitted at a given reporting rate, the frequency and ROCOF values computed sample-by-sample can be averaged over one reporting period to mitigate the detrimental impact of wideband noise.

E. Computational complexity evaluation

In principle, the computational complexity of the overall algorithm depends on the sum of the complexity of the three main steps summarized at the beginning of Section III, i.e., RMT-based narrowband components detection, ESPRIT-based frequency estimation of such detected components and IpD2FT-based synchrophasor estimation.

- The computational complexity of the detection algorithm of possible narrowband components is dominated by (7) and by the subsequent SVD computation. The former task requires $O\left(LM^2\right)$ operations, while the complexity of SVD is $O\left(M^3\right)$. The complexity of the RMT-based hypotheses testing algorithm can be hardly estimated exactly, as it depends on the time spent in the innermost loop to determine $\hat{\sigma}^2_{RMT|\hat{D}}$ at every iteration. Assuming that the solutions of the second-degree equation (9) are computed by using closed-form expressions (namely with a negligible computational burden), the complexity of (8)-(9) is just slighlty greater than $O\left(M+2\hat{D}\right)$, where $\hat{D}$ is increased from 1 to *D*. Since the iterative estimator $\hat{\sigma}^2_{RMT|\hat{D}}$ based on (8)-(9) requires about 10 iterations to converge to a steady value, the overall computation complexity of the innermost loop for noise variance estimation is about $O\left(10\left(M+D+1\right)\right)$. The computation of the threshold value through (10) has a negligible computational cost once the input parameters are given. However, in principle *D* hypothesis testing must be performed before the null hypothesis H_0 is accepted. Therefore, the overall order of complexity of the RMT-based detection step is approximately $O\left(10D\left(M+D+1\right)\right)$. Ultimately, the complexity of the whole first stage of the proposed algorithm is $O\left(LM^2+M^3+10D\left(M+D+1\right)\right)$. Obviously, the weight of the last term is usually negligible compared with the other two, because in practice $D << M$.
- The complexity of the ESPRIT-based frequency estimator depends on the number of operations in (15) and on the subsequent eigenvalue computation. Assuming that all narrowband components are detected (i.e., $\hat{D} = D$), expression (15) requires to perform three matrix products between matrices of size $2D \times M$ and $M \times 2D$, and the computation of an inverse matrix of size $2D \times 2D$. Thus, the overall complexity to compute (15) is $O\left(12D^2\left(M-1\right)+8D^3\right)$. The eigenvalue decomposition of the resulting $\hat{\mathbf{\Psi}}$ matrix requires further $O\left(8D^3\right)$ operations. Observe that even if the overall complexity increases cubically with D, it grows just linearly with *M*. Therefore, the computational burden of the ESPRIT-based frequency estimation step is expected to be lower than the burden for narrowband components detection.
- The IpD2FT-based synchrophasor estimation step described in Section III.D for a single set of estimates requires: $O\left(N\left(D+2\right)\right)$ operations to calculate the DFT spectral samples at the wanted frequency bins; $O\left(2N\left(D+2\right)^2\right)$ operations to determine the elements of matrices $\mathbf{W}_P\left(\hat{\mathbf{v}}\right)$ and $\mathbf{W}_I\left(\hat{\mathbf{v}}\right)$ in (20); and $O\left(8\left(D+2\right)^3+4\left(D+2\right)^2\right)$ operations to solve (20). The frequency and ROCOF estimators (21) and (22) require just a few further operations with a constant additional burden. Thus, also the complexity of the IpD2FT-based synchrophasor estimation step grows cubically with D but just linearly with *N*.

In conclusion, even if the overall computational complexity looks considerable, in practice the actual number of operations is constrained by: i) the number of narrowband components *D* (which is in the order of a few tens at most); ii) the fact that the value of *M* is constrained by both the limited PMU sampling frequency (in the order of a few kHz) and the short duration of each record (i.e., between one and two power line cycles); iii) the fact that the value of *L* should be preferably comparable with *M* to maximize detection sensitivity (further details on this crucial point are provided in Section IV). In addition to such constraints, it is of course essential to keep the value of *N* as small as possible, e.g., by collecting and processing the samples of no more than two power line cycles at a time.

IV. Simulations and Results

In order to evaluate the performance of the proposed algorithm, a three-step analysis is described in the following. Firstly, the accuracy of the RMT-based method for narrowband components detection is assessed under different conditions and it is compared with the results obtained using the AIC [29], and the MDL [30] techniques. The results of this analysis are summarized in Section IV.A. Secondly, the accuracy of the ESPRIT-based frequency estimation for the narrowband components detected with the RMT-based method is analyzed in Section IV.B. Finally, the overall estimation accuracy of the eIpD2FT algorithm (both in the M Class testing conditions specified in the IEEE/IEC Standard [1] and in the presence of a critical mixture of harmonics and OOBIs) is evaluated in Section IV.C. In this latter analysis, a comparison with the original IpD2FT estimator [13] and the TLTFT algorithm [16] is also provided. The TLTFT was chosen as a benchmark because, unlike the standard TFT approach, it embeds two additional features that enable a fairer comparison with the proposed algorithm, i.e., i) a preliminary estimation of

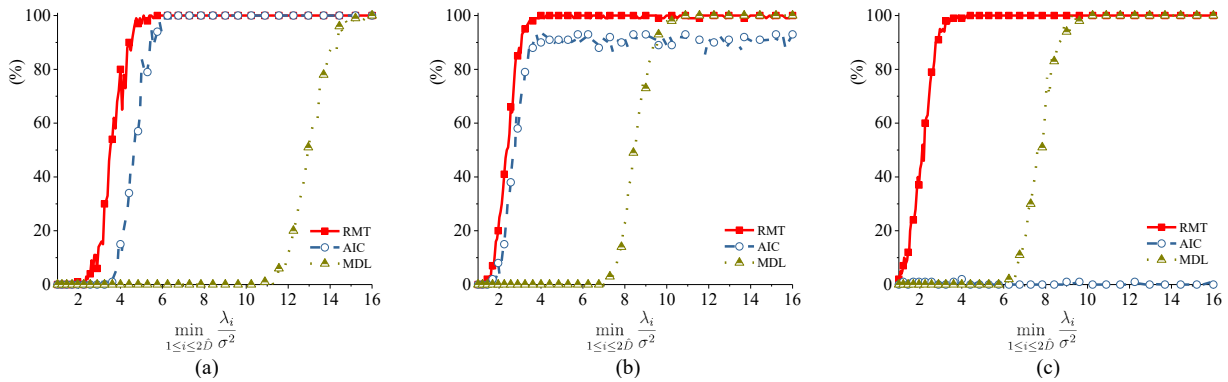

Fig. 2. Probability curves of correctly accepting the null hypothesis H_0 when the collected signals contain: (a) two interhamonics (one in the frequency band within [10 Hz,25 Hz] and another one in the band [75 Hz, 100 Hz], with the interharmonics frequency values changing randomly 100 times); (b) the first 10 harmonics; (c) the first 20 harmonics. In all cases the amplitude of the D-1 narrowband interferers is changed randomly between a given lower bound (which is increased linearly and used to label the x-axis of the probability curves) and 10% of the fundamental. The different curves in each plot refer to the RMT-based detector and the AIC and MDL model order estimators, respectively.

the fundamental frequency with a consequent adjustment of the coefficients of the system matrix; ii) a criterion to choose the number of narrowband components to be included in the signal for a given observation interval length [16].

Assuming that the PMU sampling frequency $f_s = 6.45$ kHz (i.e., large enough to avoid aliasing) and SNR=60 (considering the fundamental component only) is 60 dB [37], the values of parameters M, L, and N used to run all simulations were set to 173, 100 and 257, respectively. The rationale for this choice is the following.

As briefly explained in Section III.B, the values of M should be chosen in such a way that i) more than one power line cycle is observed and ii) the value of frequency f_s/M does not coincide with the frequency of the fundamental, of one of its harmonics or of any possible OOBI (e.g., components within [10 Hz, 25 Hz] or [75 Hz, 100 Hz] if the PMU reporting rate is 50 frames/s). The conditions i) and ii) mentioned above are met if the value of f_s/M lies within [27.5 Hz, 37.5 Hz]. Thus, the smallest possible odd value of M that satisfies such conditions results from $M = f_s/37.5 + 1 = 173$. It is explained in [34] that the asymptotic limit of detection of a narrowband component for large values of M and L is $\sigma^2\sqrt{M/L}$. Therefore, if $\sqrt{M/L} \approx 1$, namely if the value of L is not only large enough, but also comparable to M, the detection limit approximates the noise variance. Nonetheless, it was verified through simulations that, in the case at hand, the value of L can be decreased by about 40% without degrading detection performance. Thus, L was finally set to 100 to keep the computational burden as low as possible.

As far as the length of the observation intervals for synchrophasor estimation is concerned, data records of duration equal to two nominal powerline cycles plus 1 sample (so that the Taylor's series coefficients of all phasors can be computed exactly in the center of each observation interval) are considered in the following. Hence, if $f_s = 6.45$ kHz and $f_{nom} = 50$ Hz, the record length results $N = 257$ samples. Quite importantly, to the best of Authors' knowledge, no other estimation algorithms for PMUs are currently able to comply with the M Class OOBI rejection requirements of the IEEE/IEC Standard over only two-cycle-long observation intervals.

A. Performance evaluation of the RMT-based algorithm for narrowband component detection

To evaluate and to compare the narrow-band components detection capability of the RMT-based algorithm, the AIC technique and the MDL estimator, repeated Monte Carlo simulations were performed in three different scenarios, i.e., by including: (a) two interhamonics (one in the frequency band within [10 Hz, 25 Hz] and another one in the band [75 Hz, 100 Hz], with the interharmonic frequency values changing randomly 100 times in the selected bands); (b) the first 10 harmonics and (c) the first 20 harmonics. In every scenario, the minimum ratio between the smallest eigenvalue of the narrowband components and the noise variance was increased linearly between 1 (which represents the ideal asymptotic limit of detection when $M, L \to \infty$) and 16. For every value of this ratio, 500 detection tests were performed by changing randomly the amplitude of the D-1 narrowband interferers up to reach 10% of the fundamental (namely the M Class relative maximum amplitude of harmonics and interharmonics specified in the IEEE/IEC Standard). Based on the results of such tests, the probability of correctly detecting the actual number of narrowband components was computed. The probability curves obtained in the three scenarios mentioned above with the RMT-based algorithm for β=0.01 (solid lines), the AIC technique (dashed lines) and the MDL estimator (dotted lines) are shown in Fig. 2(a)-(c), respectively.

It is quite evident that in all analyzed cases the detection threshold of the RMT-based technique is lower than the thresholds of the other estimators (particularly the MDL one). Moreover, the AIC techniques seems to be very sensitive to the number of narrowband components. Therefore, it is not robust when the amount of narrowband interferers grows. On the other hand, when the RMT-based algorithm is used, the narrowband components are correctly detected with a 99% level of confidence when the minimum ratio λ_j / σ^2 for j=1,…,2D+1 ranges between about 3.5 and 4.5. Recalling that in (6) $\lambda_j = \frac{M}{4} \cdot A_j^2$, it follows that, if SNR=60 dB and M = 173 samples, the minimum detectable amplitude of a narrowband

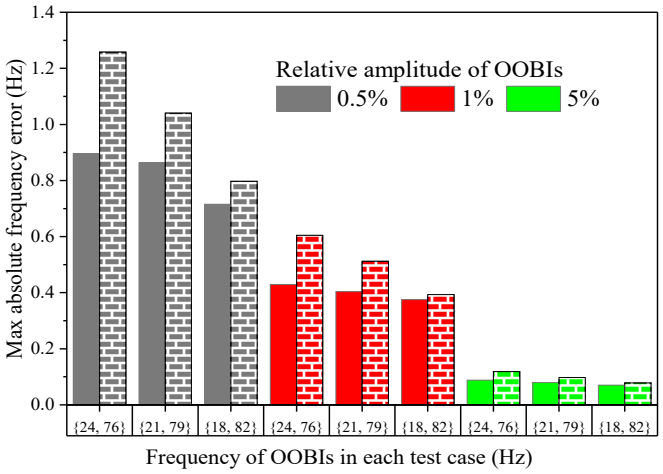

Fig. 3. Maximum absolute frequency estimation errors of different pairs of OOBIs obtained at the output of the ESPRIT stage. The OOBIs frequencies are symmetrically chosen below (solid bars) and above (brick-patterned bars) the fundamental one. Different colors refer to different OOBI amplitude values (0.5%, 1% and 5%).

component is about 0.2% of the fundamental component, i.e., small enough to assume that the impact of the missed detection of such interferers on synchrophasor estimation is negligible.

B. Accuracy of the frequency estimation for the narrowband interferers

The accuracy of the ESPRIT-based frequency estimation of the detected quasi-stationary narrowband components is rather important, as it also affects the uncertainty of the elements of the system matrix in (20). Such accuracy has been assessed by multiple Monte Carlo simulations performed in two different scenarios. In the former one, two OOBIs (one in the frequency band [10 Hz, 25 Hz] and another one within [75 Hz, 100 Hz]) are overlapped to the fundamental component. In the second set of simulations, the 2nd, 3rd, 4th, and 5th harmonics are subsequently added to the fundamental. In both cases, 500 simulation runs were performed assuming that the initial phase of the various narrowband components is randomly chosen in [0, 2π) and that their relative amplitude with respect to the fundamental is 0.5% (i.e., just slightly above the detection threshold), 1% (intermediate size) or 5% (i.e., large enough to be regarded as critical). In order to take the frequency deviation of the fundamental into consideration, the fundamental frequency is also changed randomly with uniform distribution in the band [45 Hz, 55 Hz]. The individual maximum absolute frequency errors associated to each pair of OOBIs and those associated with different harmonics are shown in Fig. 3 and Fig. 4, respectively. In both Figures, the frequency estimation errors related to the fundamental are purposely not shown because: i) they would be hardly visible, since they are orders of magnitude lower than the reported ones; ii) they are superseded by the results of the cascaded IpD2FT dynamic estimator, which will be shown in Section IV.C.

In all cases, the ESPRIT-based frequency estimation accuracy increases when the relative amplitude of either OOBIs or harmonics also grows. This is rather important, because it

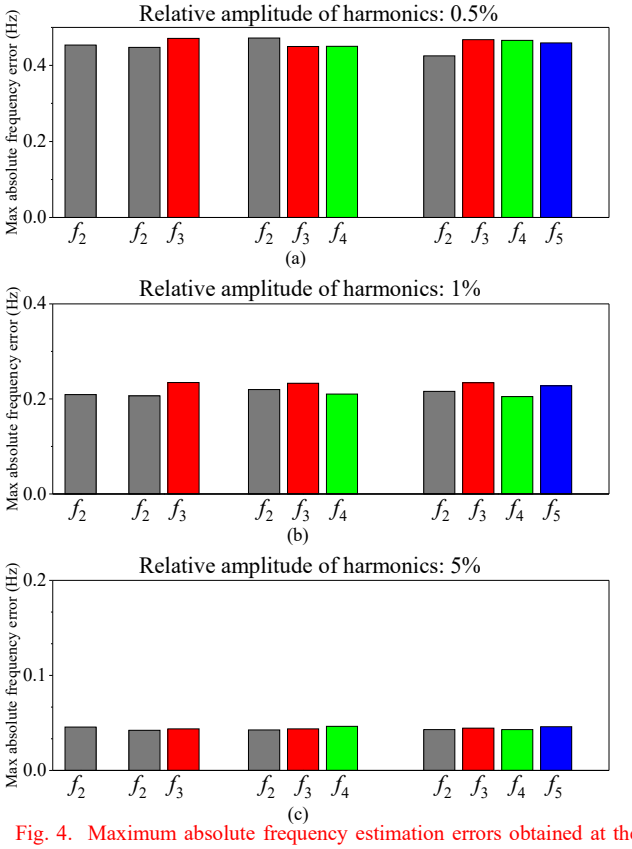

Fig. 4. Maximum absolute frequency estimation errors obtained at the output of the ESPRIT stage when an increasing number of harmonics (from the 2nd to the 5th) affect the fundamental component. The bar diagrams in (a), (b) and (c) refer to harmonics of amplitude equal to 0.5%, 1% and 5% of the fundamental, respectively.

implies that the elements of the system matrix in (20) are computed with greater accuracy, when the disturbances perturbing the synchrophasor estimation become more severe.

Figs. 3 and 4 provide also some further complementary information. In particular, the results in Fig. 3 show clearly (and quite reasonably) that the frequency estimation accuracy in the presence of multiple OOBIs tends to degrade as the spectral distance between them and the fundamental decreases. Fig. 4 confirms instead that estimation accuracy of multiple harmonic frequencies is rather insensitive to their number.

C. Overall estimation results and accuracy analysis

In the following, the M Class testing conditions specified in the IEEE/IEC Standard to evaluate the accuracy of the overall eIpD2FT algorithm are listed and briefly recalled.

- *Test a (Fdev only):* Off-nominal frequency deviations ranging from -5 Hz to 5 Hz;
- *Test b (Fdev+harm)*: Off-nominal frequency deviations ranging from -5 Hz to 5 Hz, and harmonic distortion obtained by including one harmonic at a time from the 2nd up to the 50th one, with amplitude equal to 10% of the fundamental.
- *Test c (OOBI only)*: A single OOBI interferer of amplitude equal to 10% of the fundamental and frequency increasing by 1 Hz at a time within intervals [10 Hz, 25 Hz] and [75 Hz, 95 Hz].
- *Test d (AM)*: Amplitude modulation with modulation index 0.1 and modulating tone frequency up to 5 Hz.

TABLE II

MAXIMUM TVE, |FE| AND |RFE| VALUES RETURNED BY THE EIPD2FT, IPD2FT AND TLTFT ALGORITHMS OVER 2-CYCLE-LONG OBSERVATION INTERVALS IN DIFFERENT TESTING CONDITIONS. ALL OF THEM, EXPECT THE LAST ONE, ARE SPECIFIED IN THE IEC/IEEE STANDARD. IN ALL CASES, THE HANN WINDOW IS USED AND *SNR* = 60 DB. THE LIMITS OF THE IEC/IEEE STANDARD (WHEN DEFINED) ARE ALSO SHOWN FOR COMPARISON.

		maxTVE (%)				**maxFE (mHz)**				**maxRFE (Hz/s)**			
Test case		**Std limit**	**eIpD2FT**	**IpD2FT**	**TLTFT**	**Std limit**	**eIpD2FT**	**IpD2FT**	**TLTFT**	**Std limit**	**eIpD2FT**	**IpD2FT**	**TLTFT**
a	*Fdev only*	1	0.06	0.06	0.07	5	0.3	0.3	0.3	0.1	0.07	0.07	0.07
b	*Fdev+harm*	1	0.07	5.58	0.10	25	1.2	$>10^2$	1.6	-	0.32	$>10^2$	0.46
c	*OOBI only*	1.3	0.12	9.99	10.1	10	1.6	$>10^2$	$>10^2$	-	0.42	$>10^2$	$>10^2$
d	*AM*	3	0.07	0.07	0.06	300	9.4	9.9	7.0	14	2.2	2.2	1.8
e	*PM*	3	0.07	0.07	0.05	300	11.7	13.2	14.3	14	2.4	1.9	1.5
f	*F ramp*	1	0.07	0.07	0.07	10	0.7	0.7	0.7	0.2	0.18	0.18	0.18

TABLE III

MAXIMUM SYNCHROPHASOR, FREQUENCY AND ROCOF RESPONSE TIMES OBTAINED WITH EIPD2FT, IPD2FT AND TLTFT ALGORITHMS OVER 2-CYCLE-LONG OBSERVATION INTERVALS DURING STEP CHANGE TESTS. THE M CLASS LIMITS SPECIFIED IN THE IEEE/IEC STANDARD ARE ALSO SHOWN FOR TH COMPARISON.

		Synchrophasor response time (cycles)				**Frequency response time (cycles)**				**ROCOF response time (cycles)**			
Test case		**Std limit**	**eIpD2FT**	**IpD2FT**	**TLTFT**	**Std limit**	**eIpD2FT**	**IpD2FT**	**TLTFT**	**Std limit**	**eIpD2FT**	**IpD2FT**	**TLTFT**
g	*Amp step*	7	0.7	0.7	0.9	14	2.7	2.6	2.8	14	2.8	2.8	2.9
h	*Phase step*	7	1.2	1	1.3	14	2.7	2.6	2.7	14	2.8	2.8	2.8

- *Test e (PM):* Phase modulation with modulation index 0.1 rad and modulating tone frequency up to 5 Hz.
- *Test f (F. ramp)*: Frequency ramps increasing or decreasing at ±1 Hz/s within f_{nom}±5 Hz.
- *Test g (Amp. step)*: ±10% amplitude step changes.
- *Test h (Phase step)*: ±π/18 phase step changes.

To enable a fair comparison between the proposed algorithm, the original IpD2FT estimator and the TLTFT technique, the classic Hann window was adopted in all cases, as it provides a good trade-off between spectral main-lobe width and long-range spectral leakage suppression capability.

The maximum values of Total Vector Error (TVE),

$$TVE = \left| \frac{A_1(0)e^{j\varphi_1(0)} - \hat{p}_{1,0}}{A_1(0)e^{j\varphi_1(0)}} \right|, \tag{23}$$

absolute Frequency Error (FE)

$$|FE| = \left| f_1 - \hat{f}_1 \right| \tag{24}$$

and absolute ROCOF errors (RFE),

$$|RFE| = \left| ROCOF - \widehat{ROCOF} \right| \tag{25}$$

obtained in the *Tests a* to *f* are reported in Table II. The response time values obtained in *Tests g* and *h* (namely the time intervals between the instants at which the measured values of synchrophasor, frequency or ROCOF as a result of a fundamental amplitude or phase step change exceed 1%, 5 mHz or 0.1 Hz/s, respectively, and the time after which the measured values steadily remain under such thresholds) are instead reported in Table III. The IEEE/IEC Standard limits for a reporting rate of 50 frames/s are also shown for the sake of comparison. The reported values are computed over 200 repeated tests by changing randomly the initial phase of all sinusoidal components with uniform probability within $[0, 2\pi)$.

In the case of *Test a*, the estimation accuracy of all estimators is basically almost the same, as expected since no narrowband interferers are present. The only difference is that the original IpD2FT estimates the off-nominal frequency deviation iteratively, whereas the eIpD2FT and TLTFT algorithms estimate the fundamental frequency through ESPRIT and a preliminary IpDFT, respectively.

In the case of *Test b*, the eIpD2FT and the TLTFT algorithms provides much better results than those of the original IpD2FT estimator, because the former two algorithms estimate the harmonics (particularly the 2nd and 3rd one which are the most critical), while the original IpD2FT does not and, in addition, the results over two-cycle-long intervals are strongly affected by the spectral leakage of the 2nd harmonic, which is the main responsible of the large values shown in Table II.

In the case of *Test c*, even TLTFT accuracy strongly degrades due to the fact that the OOBIs are not included in the model. On the contrary, the proposed eIpD2FT approach provides much more accurate results than the other techniques and full compliance with M Class requirements thanks to the reliable OOBIs detection and to the estimation of the corresponding phasors.

In the AM and PM tests (*Tests d* and *e*), all algorithms exhibit

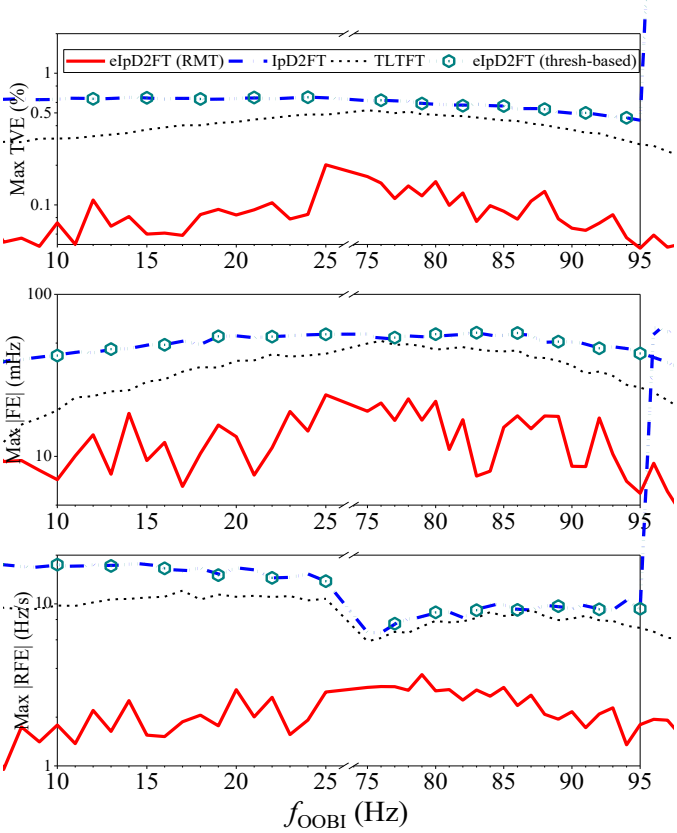

Fig. 5. Maximum TVE, |FE| and |RFE| values obtained with the eIpD2FT, the IpD2FT and the TLTFT algorithms over two-cycle-long observation intervals as a function of the 0.5% OOBI frequency f_{OOBI}, when an additional 0.5% second-order harmonic is included in the signal model.

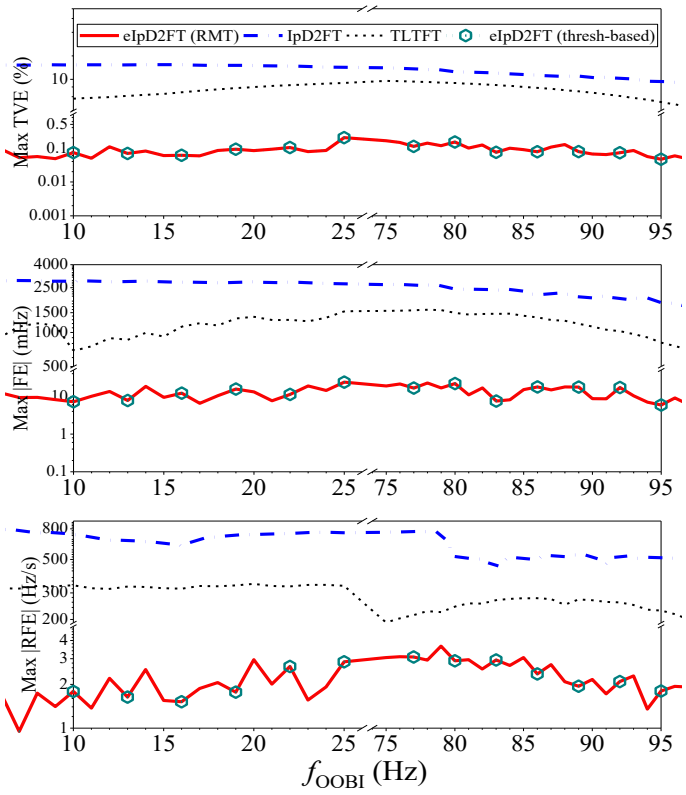

Fig. 6. Maximum TVE, |FE| and |RFE| values obtained with the eIpD2FT, the IpD2FT and the TLTFT algorithms over two-cycle-long observation intervals as a function of the 10% OOBI frequency f_{OOBI}, when an additional 10% second-order harmonic is included in the signal model.

comparable accuracy. This is due to the fact that possible in-band oscillations close to the fundamental tone are not recognized by the eIpD2FT as narrowband interferers. Therefore, they are not used to increase the size of (19). As a consequence, the eIpD2FT and the original IpD2FT algorithm rely on a linear system with the same size, like in the case of *Test a*. In addition, the use of a common Taylor's series synchrophasor model truncated to the second order makes the three estimation algorithms rather equivalent. The same behavior can be observed in the case of *Test f*, since the linear frequency change of the frequency ramp test is so slow that the waveforms collected over two-cycle observation intervals can be regarded as quasi static. In conclusion, in the testing conditions *d*, *e* and *f*, the three algorithms exhibit almost the same accuracy.

In the amplitude and phase step changes tests (*Tests g* and *h*), the response times of three algorithms are also almost the same and they are well below the limits specified in the IEEE/IEC Standard due to the short (i.e., two-cycle-long) observation intervals.

In order to highlight the benefits of the eIpD2FT algorithm with respect to the original IpD2FT and the TLTFT estimators, two further tests (not included in Table II) involving multiple narrowband components were performed. The first one is an extension of *Test b* in which the harmonics from the 2nd to the 10th (all with amplitude equal to 10% of the fundamental) have been progressively included into (1). Again, the static off-nominal frequency deviations are swept linearly from -5 Hz to 5 Hz. The corresponding maximum TVE, |FE| and |RFE| values obtained with the eIpD2FT algorithm are: 0.07, 3.4 mHz and 1.8 Hz/s, respectively. Such results are slightly better than those obtained with the TLTFT algorithm (i.e., 0.13, 6.1 mHz and 2.2 Hz/s) and, not surprisingly, they are much better than those returned by the original IpD2FT, which are still dominated by the spectral infiltration of the 2nd harmonic.

A further testing condition was derived from *Test c* by adding the 2nd harmonic to the OOBI. Two extreme cases were considered in this kind of tests. In the former one, both narrowband disturbances are very small, i.e., with amplitude equal to 0.5% of the fundamental. In the latter one, they are instead rather large, i.e., with relative amplitude equal to 10% of the fundamental. The former condition aims at showing the higher sensitivity of the RMT-based algorithm to narrowband component detection and the consequent benefits on synchrophasor, frequency and ROCOF estimation. The latter one is instead conceived to further investigate the robustness of the overall algorithm. In both cases, the OOBI frequency is varied within bands [10 Hz, 25 Hz] and [75 Hz, 95 Hz]. The corresponding maximum TVE, |FE| and |RFE| values are shown in Figs. 5 and 6, respectively. Different line styles refer to different estimators, i.e., the proposed RMT-based eIpD2FT algorithm (solid lines), the basic IpD2FT estimator (dash-dotted lines), the TLTFT estimator (dotted lines) and the

preliminary eIpD2FT algorithm with a threshold-based based on a heuristic threshold [15].

Observe that under the effect of mild interferers (Fig. 5), the original threshold-based eIpD2FT yields the same results as the IpD2FT, because it is unable to detect the narrowband components of amplitude 0.5%. On the contrary, the RMT-based eIpD2FT algorithm returns the lowest TVE, |FE| and |RFE| values.

Under the effect of strong interferers instead (Fig. 6), the RMT-based eIpD2FT algorithm returns the same results as the original threshold-based eIpD2FT, because both of them are able to detect the narrowband interferers correctly. In this case, both solutions return TVE, |FE| and |RFE| values that are from one to some orders of magnitude lower than those achieved with the IpD2FT and TLTFT estimators.

A final point that deserves attention is a comparison of the computational complexity of the four algorithms involved in the analysis. Of course, the RMT-based algorithm exhibits the largest computational complexity. As explained in Section III.E, this grows cubically with *M* and *D*, but just linearly with *N*. The computational complexity of the original threshold-based eIpD2FT algorithm, although roughly comparable, is a bit lower since the RMT-based detection step (whose complexity is $O\left(10D\left(M+D+1\right)\right)$) is replaced by a plain comparison between the singular values of matrix $\hat{\mathbf{R}}$ and the heuristic threshold computed a priori.

The computational complexity of the original IpD2FT algorithm is almost the same as that of the last step of the RMT-based algorithm only. However, two important differences exist: i) the number of narrowband components in the original IpD2FT was implicilty assumed to be one, and ii) the system of equation (20) must be solved iteratively a few times to compensate for the effect of possible off-nominal frequency deviations. Thus, the overall computational complexity is $O\left(I\cdot N\right)$, where I denotes the number of iterations required by the algorithm to converge.

Finally, based on what reported in [16], the TLTFT estimator consists of two stages: an initial IpDFT applied to the filtered data record to extract the off-nominal frequency deviation of the fundamental tone and a weighted least-squares estimator. The computational complexity of the first stage is $O\left(N\right)$. In the second stage, up to four harmonics are included in the signal model when two-cycle-long intervals are considered and the overall complexity is $O\left(N^2\right)$. Therefore, the computational complexity of this synchrophasor estimator per se is expected to be higher than that of the last stage of the RMT-based eIpD2FT. However, the processing burden of the RMT-based technique is dominated by the $\hat{\mathbf{R}}$ estimation and the SVD computation.

V. Conclusions

In this paper, an enhanced version of the IpD2FT (eIpD2FT) for synchrophasor estimation is presented and characterized. By utilizing a non-parametric hypotheses testing algorithm based on random matrix theory, the potential multiple narrowband components in the input signal can be detected with a high level of confidence, thus adapting the size of both the ESPRIT-based frequency estimator and the IpD2FT-based synchrophasor estimator to the actual number of harmonics and interharmonics. The chosen narrowband components detector exhibits superior sensitivity and robustness compared with other state-of-the-art solutions for model order estimation. In addition, the cascaded synchrophasor estimator exhibits higher accuracy than both the original IpD2FT and the techniques based on the Taylor Fourier Transform. As a consequence, the eIpD2FT algorithm ensures full compliance with the M Class PMU requirements defined in the IEEE/IEC Standard 60255-118-1:2018 (particularly the out-of-band interharmonics test) even when just two-cycle-long observation intervals are acquired and processed. Such results are preserved when either multiple harmonics or a mixture of harmonics and interharmonics is added to the fundamental component, as it may happen in the case of voltage or current waveforms affected by severe nonlinear distortion.

References

[1] "IEEE/IEC International Standard - Measuring relays and protection equipment - Part 118-1: Synchrophasor for power systems - Measurements," *IEC/IEEE 60255-118-1:2018,* pp. 1-78, 2018.

[2] D. Macii and D. Petri, "Digital Filters for Phasor Measurement Units: Design Criteria, Advantages and Limitations," in *2019 IEEE 10th International Workshop on Applied Measurements for Power Systems (AMPS)*, 2019, pp. 1-6.

[3] A. J. Roscoe, I. F. Abdulhadi, and G. M. Burt, "P and M Class Phasor Measurement Unit Algorithms Using Adaptive Cascaded Filters," *IEEE Transactions on Power Delivery,* vol. 28, no. 3, pp. 1447-1459, 2013.

[4] A. J. Roscoe, B. Dickerson, and K. E. Martin, "Filter Design Masks for C37.118.1a-Compliant Frequency-Tracking and Fixed-Filter M-Class Phasor Measurement Units," *IEEE Transactions on Instrumentation and Measurement,* vol. 64, no. 8, pp. 2096-2107, 2015.

[5] D. Belega and D. Petri, "Accuracy Analysis of the Multicycle Synchrophasor Estimator Provided by the Interpolated DFT Algorithm," *IEEE Transactions on Instrumentation and Measurement,* vol. 62, no. 5, pp. 942-953, 2013.

[6] H. Wen, C. C. Li, and L. Tang, "Novel Three-Point Interpolation DFT Method for Frequency Measurement of Sine-Wave," *Ieee Transactions on Industrial Informatics,* vol. 13, no. 5, pp. 2333-2338, Oct 2017.

[7] R. Ferrero, P. A. Pegoraro, and S. Toscani, "Employment of Interpolated DFT-based PMU Algorithms in Three-Phase Systems," in *2017 IEEE International Workshop on Applied Measurements for Power Systems (AMPS)*, 2017, pp. 1-5.

[8] P. Nanda, C. K. Panigrahi, and A. Dasgupta, "Phasor Estimation and Modelling Techniques of PMU- A Review," *Energy Procedia,* vol. 109, pp. 64-77, 2017/03/01/ 2017.

[9] D. Macii, D. Belega, and D. Petri, "IpDFT-Tuned Estimation Algorithms for PMUs: Overview and Performance Comparison," *Applied Sciences,* vol. 11, no. 5, p. 2318, 2021.

[10] F. J. Harris, "On the use of windows for harmonic analysis with the discrete Fourier transform," *Proceedings of the IEEE,* vol. 66, no. 1, pp. 51-83, 1978.

[11] D. Macii, D. Petri, and A. Zorat, "Accuracy Analysis and Enhancement of DFT-Based Synchrophasor Estimators in Off-Nominal Conditions," *IEEE Transactions on Instrumentation and Measurement,* vol. 61, no. 10, pp. 2653-2664, 2012.

[12] D. Belega, D. Macii, and D. Petri, "Fast Synchrophasor Estimation by Means of Frequency-Domain and Time-Domain Algorithms,"

IEEE Transactions on Instrumentation and Measurement, vol. 63, no. 2, pp. 388-401, 2014.

[13] D. Petri, D. Fontanelli, and D. Macii, "A Frequency-Domain Algorithm for Dynamic Synchrophasor and Frequency Estimation," *IEEE Transactions on Instrumentation and Measurement,* vol. 63, no. 10, pp. 2330-2340, 2014.

[14] A. Bashian, D. Macii, D. Fontanelli, and D. Petri, "A Tuned Whitening-Based Taylor-Kalman Filter for P Class Phasor Measurement Units," *IEEE Transactions on Instrumentation and Measurement,* vol. 71, pp. 1-13, 2022.

[15] X. Shan, D. Macii, D. Petri, and H. Wen, "Enhanced IpD2FT-based Synchrophasor Estimation through Narrowband Interferers Compensation," in *2022 IEEE International Instrumentation and Measurement Technology Conference (I2MTC)*, 2022, pp. 1-6.

[16] P. Tosato, D. Macii, M. Luiso, D. Brunelli, D. Gallo, and C. Landi, "A Tuned Lightweight Estimation Algorithm for Low-Cost Phasor Measurement Units," *IEEE Transactions on Instrumentation and Measurement,* vol. 67, no. 5, pp. 1047-1057, 2018.

[17] D. Belega and D. Petri, "Fast procedures for accurate parameter estimation of sine-waves affected by noise and harmonic distortion," *Digital Signal Processing,* vol. 114, p. 103035, 2021/07/01/ 2021.

[18] A. Derviškadić, P. Romano, and M. Paolone, "Iterative-Interpolated DFT for Synchrophasor Estimation: A Single Algorithm for P- and M-Class Compliant PMUs," *IEEE Transactions on Instrumentation and Measurement,* vol. 67, no. 3, pp. 547-558, 2018.

[19] M. A. Platas-Garza and J. A. d. l. O. Serna, "Polynomial Implementation of the Taylor–Fourier Transform for Harmonic Analysis," *IEEE Transactions on Instrumentation and Measurement,* vol. 63, no. 12, pp. 2846-2854, 2014.

[20] J. A. d. l. O. Serna, "Dynamic Phasor Estimates for Power System Oscillations," *IEEE Transactions on Instrumentation and Measurement,* vol. 56, no. 5, pp. 1648-1657, 2007.

[21] P. Castello, R. Ferrero, P. A. Pegoraro, and S. Toscani, "Space Vector Taylor–Fourier Models for Synchrophasor, Frequency, and ROCOF Measurements in Three-Phase Systems," *IEEE Transactions on Instrumentation and Measurement,* vol. 68, no. 5, pp. 1313-1321, 2019.

[22] Z. D. Drummond, K. E. Claytor, D. R. Allee, and D. M. Hull, "An Optimized Subspace-Based Approach to Synchrophasor Estimation," *IEEE Transactions on Instrumentation and Measurement,* vol. 70, pp. 1-13, 2021.

[23] J. Song, J. Zhang, and H. Wen, "Accurate Dynamic Phasor Estimation by Matrix Pencil and Taylor Weighted Least Squares Method," *IEEE Transactions on Instrumentation and Measurement,* vol. 70, pp. 1-11, 2021.

[24] P. Banerjee and S. C. Srivastava, "A Subspace-Based Dynamic Phasor Estimator for Synchrophasor Application," *IEEE Transactions on Instrumentation and Measurement,* vol. 61, no. 9, pp. 2436-2445, 2012.

[25] M. Bertocco, G. Frigo, C. Narduzzi, C. Muscas, and P. A. Pegoraro, "Compressive Sensing of a Taylor-Fourier Multifrequency Model for Synchrophasor Estimation," (in English), *IEEE Transactions on Instrumentation and Measurement,* vol. 64, no. 12, pp. 3274-3283, Dec 2015.

[26] G. Frigo, P. A. Pegoraro, and S. Toscani, "Design of Compressive Sensing Adaptive Taylor-Fourier Comb Filters for Harmonic Synchrophasor Estimation," *IEEE Open Journal of Instrumentation and Measurement,* vol. 1, pp. 1-10, 2022.

[27] R. Roy and T. Kailath, "ESPRIT-estimation of signal parameters via rotational invariance techniques," *IEEE Transactions on Acoustics, Speech, and Signal Processing,* vol. 37, no. 7, pp. 984-995, 1989.

[28] S. Kritchman and B. Nadler, "Non-Parametric Detection of the Number of Signals: Hypothesis Testing and Random Matrix Theory," *IEEE Transactions on Signal Processing,* vol. 57, no. 10, pp. 3930-3941, 2009.

[29] M. Wax and T. Kailath, "Detection of Signals by Information Theoretic Criteria," (in English), *IEEE Transactions on Acoustics Speech and Signal Processing,* vol. 33, no. 2, pp. 387-392, 1985.

[30] K. M. Wong, Q. T. Zhang, J. P. Reilly, and P. C. Yip, "On information theoretic criteria for determining the number of signals in high resolution array processing," *IEEE Transactions on Acoustics, Speech, and Signal Processing,* vol. 38, no. 11, pp. 1959-1971, 1990.

[31] Q. T. Zhang, K. M. Wong, P. C. Yip, and J. P. Reilly, "Statistical analysis of the performance of information theoretic criteria in the detection of the number of signals in array processing," *IEEE Transactions on Acoustics, Speech, and Signal Processing,* vol. 37, no. 10, pp. 1557-1567, 1989.

[32] P. Stoica and Y. Selen, "Model-order selection: a review of information criterion rules," *IEEE Signal Processing Magazine,* vol. 21, no. 4, pp. 36-47, 2004.

[33] N. El Karoui, "A rate of convergence result for the largest eigenvalue of complex white Wishart matrices," *Annals of Probability,* vol. 34, no. 6, pp. 2077-2117, Nov 2006.

[34] S. Kritchman and B. Nadler, "Determining the number of components in a factor model from limited noisy data," *Chemometrics and Intelligent Laboratory Systems,* vol. 94, no. 1, pp. 19-32, Nov 2008.

[35] I. M. Johnstone, "On the distribution of the largest eigenvalue in principal components analysis," *Annals of Statistics,* vol. 29, no. 2, pp. 295-327, Apr 2001.

[36] D. Macii, D. Fontanelli, G. Barchi, and D. Petri, "Impact of Acquisition Wideband Noise on Synchrophasor Measurements: A Design Perspective," *IEEE Transactions on Instrumentation and Measurement,* vol. 65, no. 10, pp. 2244-2253, 2016.

[37] L. Zhan, Y. Liu, J. Culliss, J. Zhao, and Y. Liu, "Dynamic Single-Phase Synchronized Phase and Frequency Estimation at the Distribution Level," *IEEE Transactions on Smart Grid,* vol. 6, no. 4, pp. 2013-2022, 2015.